Forward wound closure with regenerated silk fibroin and alginate composite bioadhesives integration of curcumin as dressings

Yanting Jing [a], Liming Ruan [b,*], Guohua Jiang [a,c,*], Yanfang Sun [d], Tianqi Liu [a], Rui Wang [a], Lei Nie [e,f], Amin Shavandi [f], Khaydar E. Yunusov [g], Uladzislau E. Aharodnikau [h]

[a] *School of Materials Science and Engineering, Zhejiang Sci-Tech University, Hangzhou, 310018, China*

[b] *Department of Dermatology, Beilun People's Hospital, Ningbo, 315800, China*

[c] *International Scientific and Technological Cooperation Base of Intelligent Biomaterials and Functional Fibers, Hangzhou, 310018, China*

[d] *College of Life Sciences and Medicine, Zhejiang Sci-Tech University, Hangzhou, Zhejiang, China*

[e] *College of Life Sciences, Xinyang Normal University, Xinyang 464000, China*

[f] *Université libre de Bruxelles (ULB), École polytechnique de Bruxelles, 3BIO-BioMatter, Avenue F. D. Roosevelt, 50 - CP 165/61, 1050 Brussels, Belgium*

[g] *Institute of Polymer Chemistry and Physics, Uzbekistan Academy of Sciences, Tashkent, 100128, Uzbekistan*

[h] *Research Institute for Physical Chemical Problems of the Belarusian State University, Minsk, 220030, Belarus*

E-mail: ghjiang_cn@zstu.edu.cn (G. Jiang)

ruandawn@126.com (L. Ruan)

Abstract: It is importnat to treat a bacterial-infected wound with a hydrogel dressing due to its excellent biocompatibility and extracellular matrix mimicking structure. In this work, we have successfully developed new antibacterial curcumin nanoparticles (Cur-NPs) loaded SF/SA composite hydrogel for wound healing. The as-prepared composite exhibited excellent biocompatibility and antibacterial activity against *E. coli* and *S. aureus in vitro*. In addition, this composite hydrogel showed good tissue adhesive strength because of its higher viscosity and abundance of amino groups distributed on SF which can form multi-aldehyde polysaccharides with the tissue surface. The porous 3D structure of the composite hydrogel facilitated the absorption of exudate from the wound site and promoted the fusion of cellular nutrients and metabolites. In the full-thickness skin defect model with and without bacterial infection, the Cur-NPs loaded SF/SA composite hydrogel prominently improves the closure of bacterial-infected wounds by improving cell proliferation, anti-inflammatory properties, vascular remodeling, and collagen deposition.

Keywords: composite hydrogel; wound healing; antibacterial; tissue adhesive; wound dressing

1. Introduction

Wounds caused by surgery or accident are increasing every year which require timely closure to ensure the healing of injuries. Generally, there are four stages of wound healing: inflammatory, multiplication, and remodeling phases [1]. However, conventional wound healing strategies, such as gauze, cotton, and surgical sutures, still show some obvious defects, which might cause trauma, unsatisfied tissue integration, poor adhesiveness, and the need for foreign bodies for supplemental fixation around the trauma [2]. An ideal wound dressing should have good biocompatibility, keep the wound wet and absorb exudates, provide protection to prevent infection, actively promote the wound healing process, encourages regeneration of damaged tissue, and serve as a depot for delivering drugs or other therapeutics [3,4].

Adhesion and moisture retention at the wound site as well as helping the tissue to regenerate are important factors in skin wound healing. ~~Hydrogel is a soft material with adjustable physical and chemical properties that possesses a 3D network structure that can absorb and retain large amounts of water in the network [5,6].~~ Tissue adhesive hydrogels can fill wounds and stop bleeding [7,8]. Therefore, biocompatible hydrogel wound dressings with bio-adhesion abilities and tissue repairabilities are required.

Silk fibroin (SF) extracted from silkworm cocoon is a biomolecular material with no immunogenicity, good biodegradation, and controllable mechanical properties, which can be directly used in clinical tissue repair to promote cell adhesion, wound

contraction, re-epithelialization and angiogenic collagen formation [9-11]. However, single-component SF hydrogels also face some inherent drawbacks, particularly their weak mechanical properties and fast degradation [12]. As a wound dressing, combining it with other polymers is an effective way to improve its adhesion, and enhance bioactivity, stability, and other biological properties. Sodium alginate (SA) is a biocompatible polysaccharide with fluid absorption capacity [13-15]. Due to its safety, stability, and fast biodegradation properties, it is commonly used as an excipient in the pharmaceutical industry [16-18]. In addition, the existence of divalent and multivalent metal ions, especially calcium ions, allows alginate-based hydrogels to be stabilized in the system, providing an equilibrium between cytocompatibility and mechanical binding strength [19].

Although the microenvironment of hydrogel is relatively moist and suitable for tissue cell migration and proliferation, bacteria still can penetrate the tissue interior through its porous structure. To improve the antimicrobial properties of hydrogel wound dressings, metal nanoparticles, such as silver ions [20,21] or antimicrobial peptides [22], could be used to enhance the antimicrobial capacity of the hydrogels. Curcumin (Cur) is an acidic polyphenolic compound extracted from the rhizome with good antioxidant, anti-inflammatory, and antibacterial properties [23,24]. However, the poor solubility and chemical stability of Cur in water limits its effectiveness at the target site or wound tissue [25,26]. Therefore, Cur needs to be fabricated into a more stable product to enhance bioavailability.

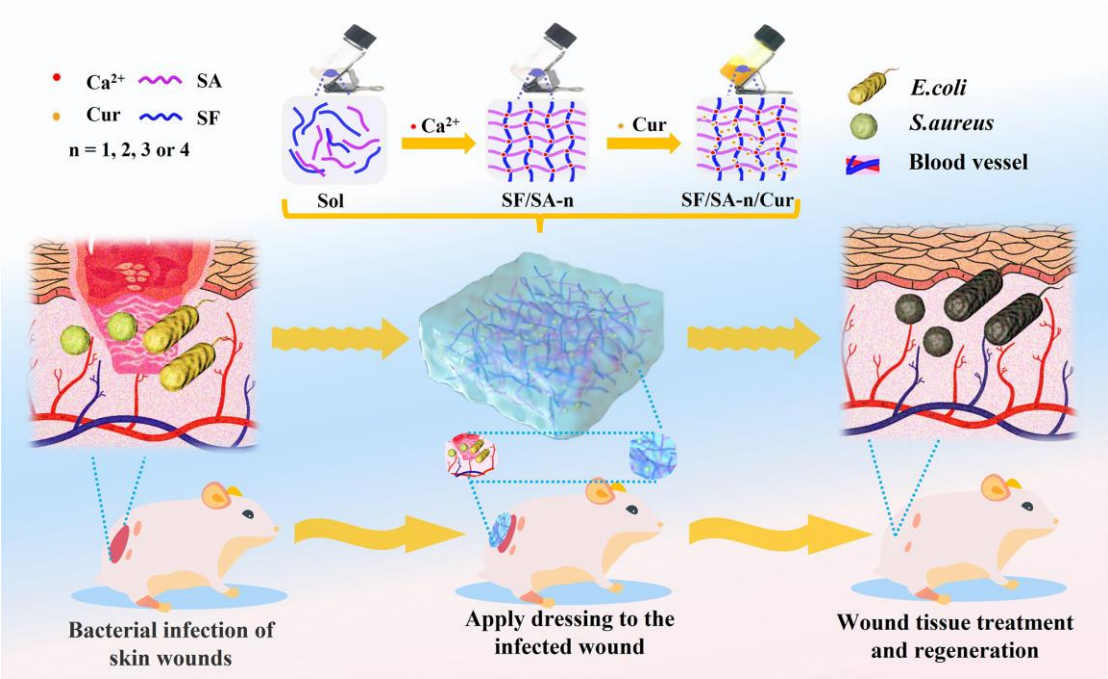

Fig. 1 Schematic illustration for the fabrication process of curcumin nanoparticles (Cur NPs)-loaded silk fibroin and alginate (SF/SA) composite bioadhesives hydrogel scaffold for wound healing.

With this background, the present study reports the composite hydrogel systems consisting of SF and SA as hydrogel scaffolds loaded with Cur nanoparticles. As shown in Fig. 1, calcium ion (Ca^{2+}) is used as a cross-linking agent to coordinate with the SF and SA chains to form a three-dimensional (3D) hydrogel network. The active groups including -OH, -COOH and $-NH_2$ groups of the hydrogel network can also bind to the tissue surface, affording strong and reversible tissue adhesion [27]. In addition, Cur NPs were further encapsulated into the composite hydrogels to enhance the antibacterial and wound healing properties of the prepared composite hydrogels. The apparent morphology, mechanical properties, cytocompatibility, anti-inflammatory and hemolytic properties of the composite hydrogels were investigated. Eventually, the composite hydrogels were applied to a full-thickness skin defect model to evaluate their effects on the repair and regeneration of common

wounds.

2. Materials and methods

2.1 Materials

Sodium alginate (SA, AP), sodium carbonate anhydrous (Na_2CO_3, AP), lithium bromide (LiBr, 99%), calcium chloride ($CaCl_2$, 99%), pluronic F127 (99%) and curcumin (Cur, AP) were purchased from Shanghai Aladdin Biochemical Technology Co., Ltd. Calcein/PI cell activity cytotoxicity detection, H&E and Masson staining kits were obtained from Bi Yun Tian Biological Reagent Co., Ltd. Sheep erythrocyte was purchased from Nanjing Quanlong Biotechnology Co., Ltd. CD31 and IL-6 mouse antibody were obtained from Cell Signaling Technology, Inc. Animal care and experimental protocols used in this study were approved by the Animal Ethics Committee of Zhejiang Sci-Tech University (Number: 20190201).

2.2 Preparation of Cur NPs-loaded SF/SA composite hydrogels

The silk fibroin (SF) solution was prepared from mulberry silkworms [28]. Briefly, silk cocoons were cut into little blocks of around 0.5 × 0.5 cm and were boiled in the Na_2CO_3 solution (0.02 M) for 30 min (~10 wt% of Na_2CO_3 solution) to remove sericin. The dried degummed cocoon pieces were further dissolved in LiBr solution (9.3 M) for 10 min at 60 °C and then filtered with a 0.45μm filter membrane. A SF solution with a concentration of 20 wt% was obtained by dialyzing in ultrapure water for 72 h (Fig. S1). Curcumin nanoparticles (Cur NPs) were fabricated by adding curcumin powder (15 mg) into 5 mL pluronic F127 aqueous solution (10 wt%) under stirring for 30 min at 50°C [29-31]. And the final concentration of Cur NPs was

controlled at 3 wt%.

To prepare SF/SA composite hydrogels, 3.75 mL SF (~20wt%) and 15 mL SA (16.7 wt%) were mixed at room temperature. Then, the different volume 0.05 M $CaCl_2$ solution (150, 200, 250, and 300 μL) was added into 2 mL SF and SA mixture under stirring to form cross-linked composite hydrogels. The resultant composite hydrogels were named SF/SA-1, SF/SA-2, SF/SA-3, and SF/SA-4, respectively. To prepare curcumin-loaded SF/SA composite hydrogels, different volume Cur NPs solution (0, 0.5, 1.0, 1.5, and 2.0 mL) was mixed with 2 mL SF/SA-3 solution and stirred for another 30 min. And the obtained curcumin-loaded SF/SA composite hydrogels were named SF/SA-3, SF/SA-3/Cur-0.5, SF/SA-3/Cur-1.0, SF/SA-3/Cur-1.5, and SF/SA-3/Cur-2.0, respectively.

2.3 Characterization

The rheological properties of the composite hydrogels were determined by a rotational rheometer (MCR52, Austria). The morphology of Cur NPs was tested by transmission electron microscopy (TEM, JEM-2100, Japan). FT-IR spectra of silk cocoon and silk fibroin (SF) were measured by FT-IR spectroscopic analysis (Nicolet Avatar 370, Thermo Scientific, USA) with the wavenumber ranging from 500 to 4000 cm^{-1}. The morphologies of the composite hydrogels were observed by scanning electron microscope (SEM) with an acceleration voltage of 15 kV at a high vacuum (Ultra 33 FE-SEM, Carl Zeiss, Germany). The skin adhesive strength of composite hydrogels was tested by a tensile test machine (5943, USA). The size distribution and crystal state were tested by dynamic light scattering (DLS, Nano-ZSZEN3600, UK)

and X-ray diffraction (XRD, D8 discover, Germany).

2.4 Cell migration and anti-inflammation test

The effect of composite hydrogels on cell migration was investigated by a scratch test of L929 cells [32]. Briefly, L929 cells were transferred into a 6-well culture plate at a density of 1×10^5 cells per well [25,33]. A line crossing the well behind the 6-well plates was drawn with 200 μL pipette tips and the slipped cells were rinsed three times with PBS. After that, 45 μL SF/SA-3/Cur-n (n = 0, 0.5, 1.0, 1.5, and 2.0) and 1.0 mL 2% serum solution was added per well. The images of cell migration were captured on a brightfield light microscopy after incubation for 0, 16, and 24 h [34]. Image J was used to calculate the closure area and rate of the scratch fields:

$$\text{Healing ratio (\%)} = [S_{0h}-S_{th} / S_{0h}] \times 100\% \quad (1)$$

where S_{0h} is the scratch area incubated in the incubator for 0 h after scratching. S_{th} is the scratch area of incubation in the incubator after scratching.

The antibacterial effects of various hydrogels were evaluated by colony counting method against Gram-negative *Escherichia coli (E. coli)* and Gram-positive *Staphylococcus aureus (S. aureus)* [12, 35]. First, the single colony of *S. aureus* and *E. coli* were inoculated into nutrient agar medium and then transferred the bacterial solution into a shaker, which was cultured at 37°C and 220 rpm for 24 h to obtain the original bacterial solution. Then, the original bacterial solution was diluted to 1.0×10^4 CFU/mL with sterile pure water to obtain a diluent solution. 100 μL diluent solutions were seeded into a 96-well culture plate at a density of 1.0×10^4 CFU/mL per well. And 3 μL SF/SA-3/Cur-n (n = 0, 0.5, 1.0, 1.5, and 2.0) and 100 μL PBS were

added per well. Subsequently, the 96-well culture plate was kept in a CO_2 vacuum incubator at 37°C for 24 h. The number of colonies in the petri dish containing each sample was counted averaged three times, and the killing rate was calculated according to the following formula:

$$\text{Antibacterial ratio} = (N_b - N_t)\times 100\%/N_b \quad (2)$$

where N_b = number of colonies without sample, and N_t = number of colonies with samples.

2.5 Hemolytic analysis

The sterile defibrated sheep whole sheep samples were centrifuged at 3,500 rpm for 5 min. The red blood cell (RBC) pellet was rinsed thoroughly with PBS solution by centrifugation for 5 min at 1500 rpm [36,37]. The supernatant was removed and RBC was diluted in the PBS. 500 μL diluent RBC suspension (~1.0 %) was first added into a centrifuge tube, and 1.5 mL PBS and 50 mg SF/SA-3/Cur-n powder samples were further added into the tubes. The tubes were shaken own slightly and incubated at 37 °C for 60 min. Control samples of positive (1.5 mL H_2O) and negative (1.5 mL PBS) were prepared. After incubation, samples were collected by centrifugal separation at 1500 rpm for about 3 min. UV–Vis spectrometer at 545 nm was employed to measure the oxyhemoglobin absorption. The percentage of hemolysis was calculated as follows:

$$\text{Hemolysis ratio } (\%)=[(OD_t-OD_n)/(OD_p-OD_n)]\times 100\% \quad (3)$$

where OD_t, OD_n, OD_p represents the absorbance of the experimental group, the negative control group sample and the positive control group at 545 nm, respectively.

2.6 Cytotoxicity evaluation

To assess the biocompatibility of composite hydrogels, mouse embryonic fibroblast L929 cells were used to evaluate the *in vitro* cytotoxicity for manifold samples (SF/SA-3, SF/SA-3/Cur-0.5, SF/SA-3/Cur-1, SF/SA-3/Cur-1.5, and SF/SA-3/Cur-2) by the MTT approach [38]. The cells with a density of 1×10^5/mL were seeded into a 96-well culture plate and incubated in a complete medium containing 10% (v/v) fetal bovine serum and 1% (V/V) penicillin-streptomycin of 100 μL at 37 ℃ in a 5%CO_2 incubator for 12 h. Then, the medium containing 45 μL samples was replaced each 24 h. The cell viability was measured with a microplate reader at 490 nm [39]. At the same time, 1 ml mouse embryonic fibroblasts L929 solution with a concentration of 1×10^5/mL was implanted into single-well culture plates. Then, the medium containing 300 μL samples was changed every 24 h. Calcein/PI cell activity and cytotoxicity test kit was used for fluorescent staining for cell proliferation at 48 and 72 h.

2.6 Wound healing *in vivo*

To discover the underlying adhibition of composite hydrogel in skin trauma closing, the whole skin defect repair experiment was carried out on the normal and bacterial-infected SD rats [38]. First, SD rats (150g-200g) were anesthetized after one week of reproduction, and a full-thickness circular skin incision with a diameter of 12mm was created on the back. SD rats were numbered and randomly divided into 6 groups: medical gauze group (positive control group), SF/SA-3, and SF/SA-3/Cur-1.0. The rats were raised separately and allowed to get water and feed at will. Wound recovery in each mouse was recorded daily using a digital camera. Image J analysis

software was used to measure the photo wound area at least three times, and the skin wound healing rate was calculated according to the formula (4):

$$\text{Wound healing rate (\%)} = ([S_i - S_r]/S_i) \times 100\% \quad (4)$$

where S_i, S_r represent the premier wound area and present wound area, respectively. And wound healing rate over 90% can be considered the healing standard. To investigate the healing of the bacteria-infected wound, 50 μL *E. coli* and 50 μL *S. aureus* with 1×10^6 CFU/mL were coated on the wounds, and repeated coating on 3, 6, and 9 days to reinfect the wounds.

2.7 Histopathological and immunohistochemical analysis

The skin tissue of the healed wound was examined by histopathology. The wound skin tissue of rats was collected, soaked with 4% formalin solution, and embedded in paraffin. The thickness of the embedded skin tissue was about 4 μm [40]. The sections were stained with hematoxylin, eosin (H&E), and Masson trichrome staining, and detected by biological microscope (BST 500x, USB). Interleukin-6 (IL-6) and vascular factor (CD-31) were characterized by direct immunostaining sections [41].

2.8 Statistical analysis

All experimental data are expressed as the mean ± standard deviation (SD). Statistically remarkable values were assessed using t-test. When * $p < 0.05$, ** $p < 0.01$, *** $p < 0.001$, *** # $p < 0.001$ the difference was statistically significant. A p-value less than 0.05 was considered statistically significant.

3. Results and discussion

3.1 Preparation of Cur NPs-loaded SF/SA composite hydrogels

To distinguish the successful synthesis of SF, the high-quality conventional Fourier transform infrared spectroscopy (FTIR) was employed under well-controlled conditions. Fig. 1a displays the FTIR spectra of cocoons and fabricated SF in the wavenumber range of 1800-800 cm^{-1}. The peaks around 1700-1600 cm^{-1} and 1600-1500 cm^{-1} reflect the vibration of amide I and II vibrations on the secondary structures of the protein backbone, respectively. The peak at 1616 cm^{-1} in cocoons has been transformed to 1637 cm^{-1} in SF due to the intramolecular β-sheet structure of the amide I band [42]. And the absorption peaks at 1513 cm^{-1} in cocoons shift to 1516 cm^{-1} in SF, which is caused by N-H bending and C-N stretching of the β-sheet structure in the amide II band. The absorption peak of the amide III bands appears at 1235 cm^{-1} in SF, which is attributed to the random coil and/or helical conformation [42,43].

In general, the gelation behavior of the hydrogel can be monitored by a rheological analytic technique. The gelation time can be defined as the intersection of storage modulus G′ and loss modulus G″ to characterize the gelation rate [44,45]. Fig. S2 shows the rheological properties of the SF/SA composite hydrogels by adding different amounts of $CaCl_2$. No storage modulus G′ and loss modulus G″ intersect can be found in the SF/SA-1 and SF/SA-2, implying the gelation has not been fully formed due to the shortage of cross-linking agent. In the case of SF/SA-3, with adding more $CaCl_2$ solution into SF and SA mixture, G' becomes larger than G" at 24 s (Fig. 1b). It is proved that $CaCl_2$ not only acts by decreasing the cross-linking time but also contributed increasing the cross-linking degree of the composite hydrogel. However, further adding $CaCl_2$ solution into SF and SA mixture, the intersection of G′ and G″

can be expanded to 96 s. This behavior can be contributed to generating competition in the mechanism of the cross-linking reaction and hydrogels viscosity [46]. It is confirmed by the changing of hydrogel viscosity, as shown in Fig. 1c. Adding excessive $CaCl_2$ in hydrogel causes a decrease in viscosity.

Appropriate tissue adhesion property is an important parameter for wound dressing application, which can ensure rapid hemostasis, continuous drug release, and accelerated skin integrity during wound healing [47,48]. To evaluate the adhesion of SF/SA composite hydrogel, the adhesion on porcine skin was measured and the adhesion strength of SF/SA composite hydrogel was calculated as well. As shown in Fig. 1d and 1e. The two porcine skins with a width of ~ 4.6 cm are connected in a zigzag shape by SF/SA composite hydrogels. SF/SA-1 sample presents the lowest load capacity, which is only around 13 N under tensile strain at ~0.7%. By adding $CaCl_2$ to improve the crosslinking degree, it could promote the adhesion of composite hydrogel to the skin. The load capacity can be significantly increased in SF/SA-2 and SF/SA-3 samples, which can reach ~17 and 22 N, respectively. However, the adhesion strength in SF/SA-4 sample decreased slightly (about 19 N for load capacity). Similar results can be found when porcine skins (~ 2.0 cm in width) are connected in overlap for 1 cm by SF/SA composite hydrogels. The highest load capacity of ~383 N can be observed for SF/SA-3 sample due to the larger adhesion area. The higher skin tissue adhesive strength of SF/SA samples can be contributed to its higher viscosity and abundance of amino groups distributed on SF which can form multi-aldehyde polysaccharides with the tissue surface. In addition, they might stably adhere to some

active wound sites with frequent movement. Taken together, SF/SA-3 has been chosen for the next-step investigations because of the shortest gelation time and the highest viscosity.

The size and the morphology of Cur NPs were investigated using dynamic light scattering (DLS) and transmission electron microscope (TEM). The average hydrodynamic diameter of Cur NPs is decreased from 20± 1.6 nm to 5 ± 2.9 nm as increasing the concentration of pluronic F127, as shown in Fig. S3. The results reveal uniformity and monodispersity of the synthesized Cur NPs. This tri-block chain of pluronic F127 creates hydrophobic pockets to hold Cur as well as gives a hydrophilic surface property to disperse Cur NPs into SF/SA hydrogel media. Fig. 1f displays the bulk appearance of the SF/SA-3 and SF/SA-3/Cur-1.0 composite hydrogels. Digital images of inclined vials are taken after ~ 5 and 20 min of sample preparation. The gelation behavior of SF/SA-3 solution can be observed by pre-mixing of SF/SA and $CaCl_2$ solutions. In addition, the introduction of Cur NPs into SF/SA does not influence the gelation behavior of the SF/SA-3 solution. The obtained SF/SA-3/Cur-1.0 composite hydrogel is orange, and the blank SF/SA-3 hydrogel is white. The morphology of SF/SA samples was observed by SEM. As shown in Fig. 1g and 1h, the lyophilized hydrogel samples exhibit porous 3D structure on the surface and cross-section that could facilitate to absorb exudates at the wound site and promote the fusion of the cellular nutrients and metabolites as wound dressing [49].

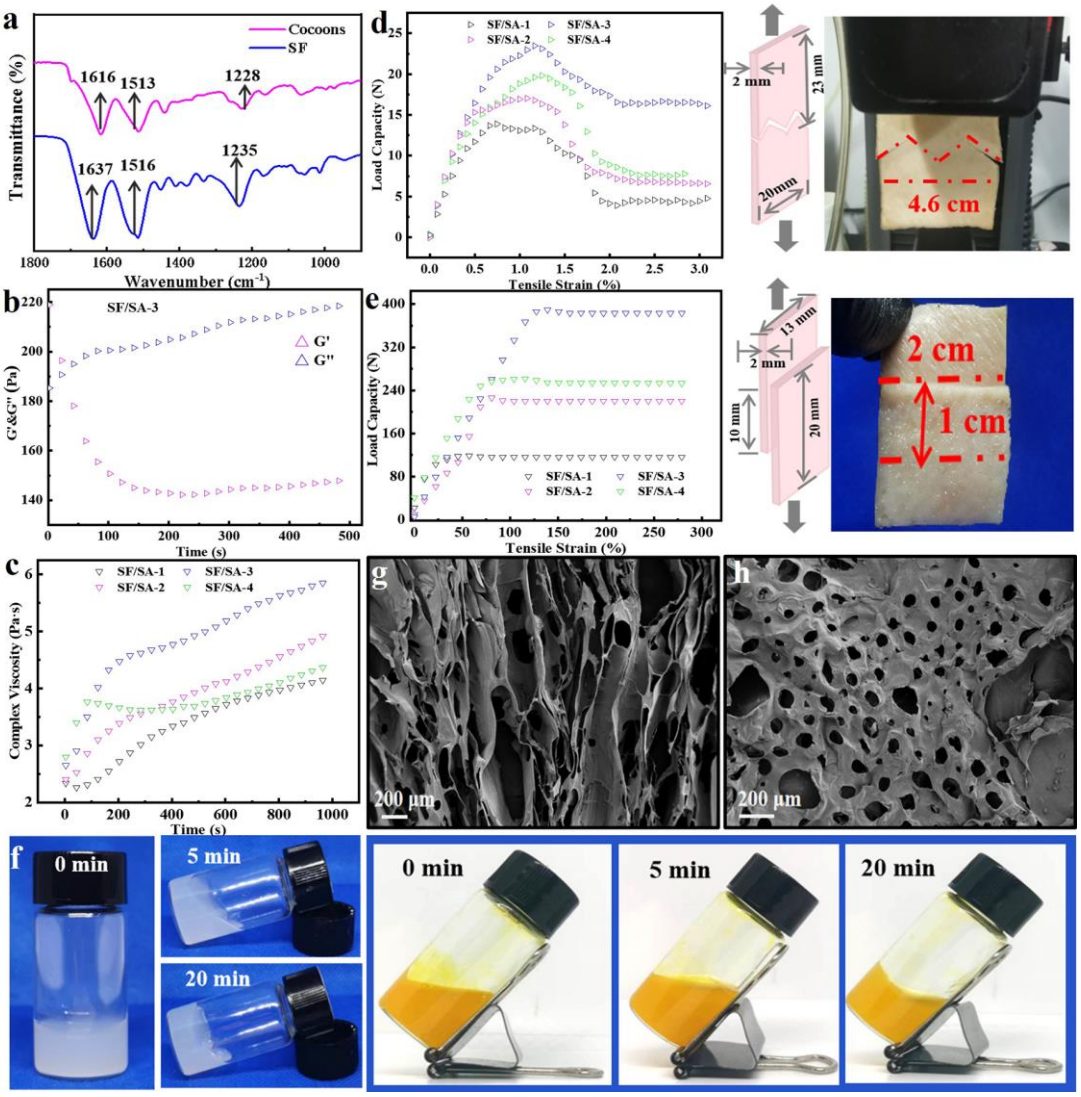

Fig. 2 FT-IR spectra of SF and cocoons (a), storage modulus G′ and loss modulus G″ (b) and viscosity (c) of composite hydrogel against mixing time, stress-strain-load curves of serrated porcine skin bonded with SF/SA-3 hydrogel and correspond schematic diagram of porcine skin for stretching (d and e), digital images of SF/SA-3 and SF/SA-3/Cur-1.0 composite hydrogels (f), and SEM images of the surface and cross-section morphologies of SF/SA-3 composite hydrogels (g and h).

3.2 Cell migration assay and antibacterial assay

Cell scratch test is a standard *in vitro* technique for cell migration research [50]. A time-dependent experiment (0-24 h) was employed to appraise the capacity of composite hydrogels to promote the expansion of L929 fibroblasts. As displayed in Fig. 3a and 3b, ~10% wound scratch area has been healed for SF/SA-3 composite hydrogels with or without Cur NPs after 16 h co-culture compared with only 2.7% for

the control group, showing a significant cell migration compared to the control (untreated) cells. After co-culture for 24 h, more than 33% wound scratch area has been healed for the SF/SA-3, SF/SA-3/Cur-0.5, and SF/SA-3/Cur-1.0 composite hydrogels. However, at higher Cur NPs concentrations in composite hydrogels, such as SF/SA-3/Cur-1.5 and SF/SA-3/Cur-2.0 composite hydrogels, the area in cell migration significantly reduced after 24 h co-culture. The results depict that, SF/SA-3 composite hydrogels with an appropriate amount of Cur NPs induced wound closure compared to the control group.

To evaluate the antibacterial activities of composite hydrogels on Gram-negative bacteria (*E. coli*) and Gram-positive bacteria (*S. aureus*), the composite hydrogels were exposed to the bacterial suspension with a concentration of 1×10^5 CFU×mL^{-1} for 24 h at 37 °C. Fig. 3c and 3d display the comparison between the control (only bacteria) group, SF/SA-3, and the composite hydrogels group. The composite hydrogels containing Cur NPs exhibit significant effects in inhibiting bacterial growth. At lower Cur NPs content (SF/SA-3/Cur-0.5), reductions for *S. aureus* and *E. Coli* could reach 23.7% and 43.4%, respectively. And more than 60% and 47% reductions for *S. aureus* and *E. Coli* can be achieved for the SF/SA-3/Cur-1.0 composite hydrogel. The inhibitory effect on *E. coli and S. aureus* can be further improved by increasing the amount of Cur NPs in composite hydrogels. These results suggest that the loading of Cur NPs in composite hydrogels is beneficial to enhancing antibacterial activity and decreasing the risk of wound infection.

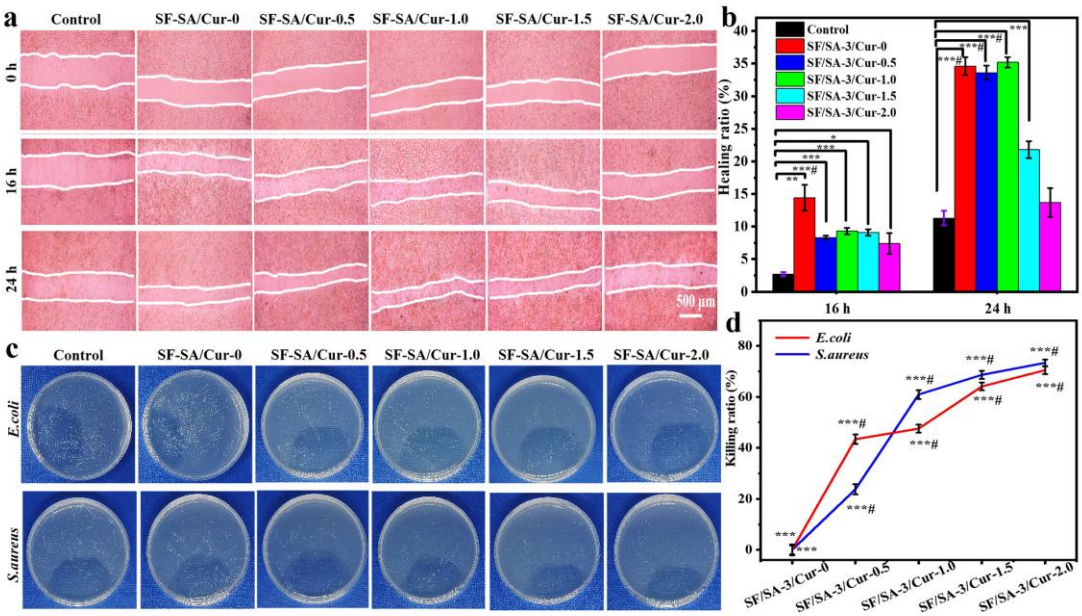

Fig. 3 Cell scratch tests against Cur NPs-loaded SF/SA-3 composite hydrogels after 0, 16, and 24 h (a), quantitative analysis of scratch healing ratio after 16 and 24 h (b), antibacterial images of Cur NPs-loaded SF/SA-3 composite hydrogels against *E. coli* and *S. Aureus* (c), and quantitative analysis of the antibacterial rate of composite hydrogels after 24 h (d).

3.3 Cytotoxicity and blood compatibility tests

A quantitative assessment of mouse embryonic fibroblast L929 cell responses toward samples are tested to evaluate the toxicity of the composite hydrogels by the MTT method. Fig. 4a and 4b illustrate the cell viability obtained by live/dead cell staining of fibroblast cells after culture 48 and 72 h. Living cells are dyed fluorescent green while dead cells are dyed fluorescent red. The confluency of the cells with SF/SA-3 composite hydrogels with or without Cur NPs was much higher as compared to the control (untreated) group. And almost no dead cells can be observed in all samples. The cell viability stays higher than 95% after 48 and 72 h co-culture with L929 cells, suggesting excellent cytocompatibility. However, at higher Cur NPs concentrations in composite hydrogels, there is a slight reduction in cell viability but no significant effect on their cytocompatibility.

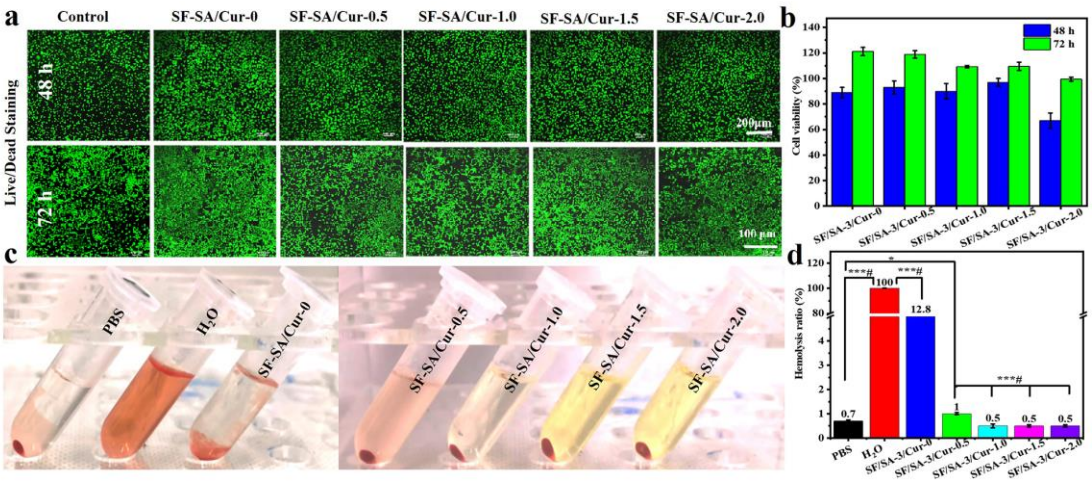

Fig. 4 Live/dead assays of L929 cultured on the surface of plastic plates with different volume ratios of Cur NPs-loaded SF/SA-3 composite hydrogels after culture for 48 and 72 h (a), MTT assay of L929 cells against Cur NPs-loaded SF/SA-3 composite hydrogels after culture for 48 and 72 h (b), hemolysis images of the composite hydrogels (c), and hemolysis rate of 1% guinea pig erythrocytes incubated with different composite hydrogels (d).

For application, biomedical materials are always inevitably in contact with blood. Hemocompatibility is critical to the blood cells activation and the beginning of wound healing [51]. The blood compatibility was further assessed to prove the biocompatibility for *in vivo* application by testing hemolytic activity. Fig. 4c and 4d exhibit the test results of determining the hemolytic potential of SF/SA composite hydrogel with different hydrogel Cur NPs load. The blood with PBS or H_2O are selected as the negative and positive control, respectively. The composite hydrogel groups all present light yellow which is similar to the blank control group. While the positive group is bright red, suggesting no hemolytic activity for erythrocytes for all composite hydrogels compared with the negative blank group.

3.4 Wound healing *in vivo*

The wound healing effect of SF/SA composite hydrogels is further assessed on the rat full-thickness skin defect model, as shown in Fig. 5a. The SF/SA composite hydrogels are directly covered on the surface of clean wound sites. Fig. 5b exhibits the

macroscopic surfaces of wounds covered with SF/SA-3, SF/SA-3/Cur-1.0, and cotton gauze. The composite hydrogels can adhere to the wound sites without secondary damage due to their excellent bioadhesive and biocompatibility. Fig. 5c and 5d show the wound area and wound healing ratio from day 1 to day 11. Compared with the cotton gauze group, both SF/SA-3 and SF/SA-3/Cur-1.0 composite hydrogels show a lower wound area and higher wound healing ratio at all various periods. After 4 days, wounds covered with the SF/SA-3 and SF/SA-3/Cur-1.0 show an improved wound healing ratio (50% and 60%, respectively) compared with cotton gauze (40%). After 11 days, the wound reduction is close to 96% and 98% in the SF/SA-3 and SF/SA-3/Cur-1.0 hydrogel groups while wound size in the control group has healed to ~85%, which demonstrates a better promotion effect on wound healing of composite hydrogels.

The histological examination was carried out on the skin wound of rats' full-thickness skin defect model with three different kinds of the wound dressing. Hematoxylin and eosin (H&E) and Masson's trichrome stainings are conducted on the regenerated skin tissues collected on Day 11. As presented in Fig. 5e, there is hardly any unmatured granulation tissue around the wound in the composite hydrogels. It is noticeable that composite hydrogel groups exhibit higher regularity for both epithelium and connective tissue, and more hair follicles and blood vessels than the control group. However, in the case of the control group, the epithelium is not intact, and the epithelial cells adjacent to the area of loss do not exhibit hyperplasia on the 11th day of post-wounding in the control group. In addition, the number of dermal

appendages in composite hydrogel groups is significantly higher than the control group (Fig. 5f).

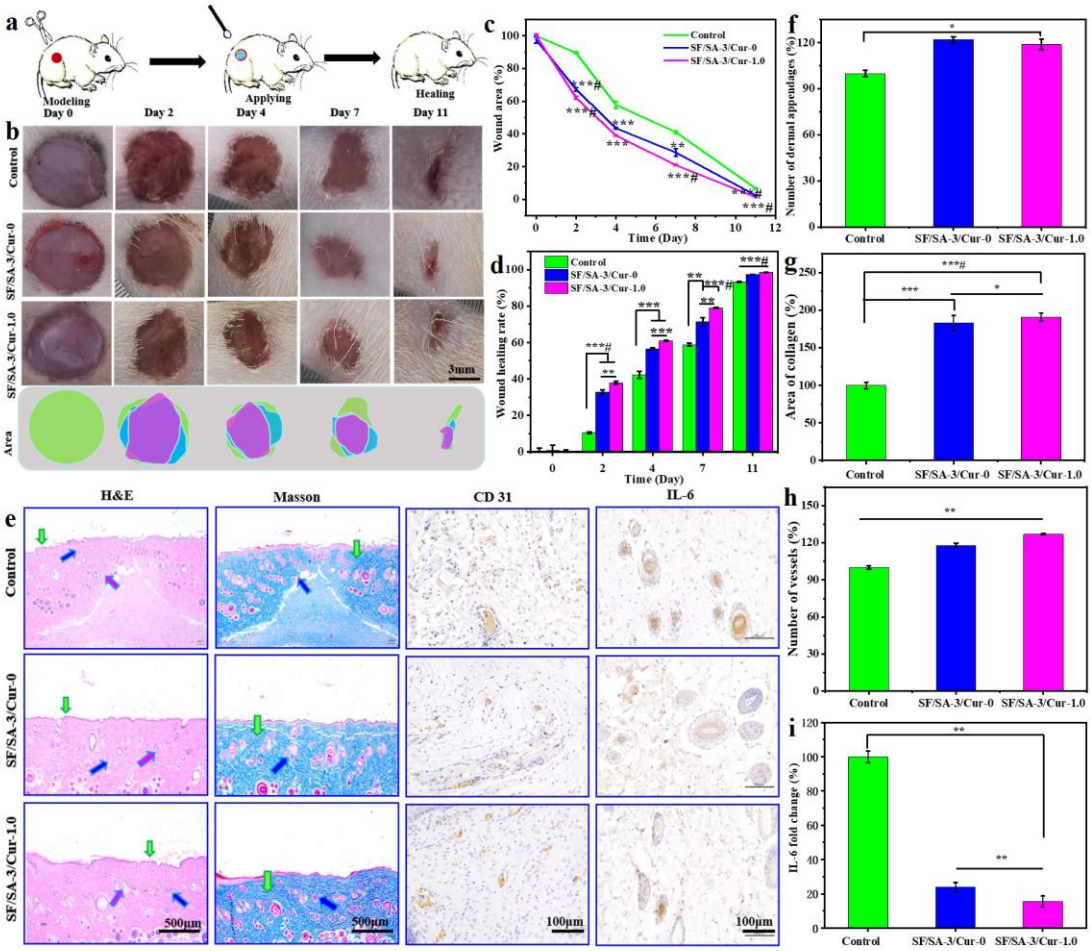

Fig. 5 Schematic illustration of clean wound healing using Cur NPs-loaded SF/SA-3 composite hydrogels as dressing (a), wound images after treated by composite hydrogels and diagram of wound size during healing (b), wound area (c) and healing rate (d) treated by composite hydrogels at days 0, 2, 4, 7 and 11. H&E and Masson's trichrome staining figures of a wound treated by composite hydrogels (e, inflammatory cells: black arrows; neovascularization: red arrows; hair follicles: green arrows; glands: yellow arrows), number of dermal appendages (f), area of collagen (g), number of vessels (h) and IL-6 secretion levels after treatment (i). * $p < 0.05$, ** $p < 0.01$, *** $p < 0.001$, ***# $p < 0.001$ vs. control group.

Masson's staining is employed to identify collagen deposition on the healing wound sites. The deposition of collagen fibers is the main feature of extracellular matrix deposition, tissue remodeling, and maturation during wound healing [52]. At the same time, it also exists a positive correlation between granulation formation and wound healing. Collagen regions reflect the formation and healing of new tissue.

Therefore, the wound healing process is closely related to the accumulation of collagen and fibrin [53]. It can be found that the wound area in the control group shows disorganized, loose collagen fibrils even 11 days of post-wounding, yet the wound with the blank SF/SA-3 composite hydrogel and Cur NPs-loaded SF/SA-3 hydrogel treatment sprouts much dense and well-arranged collagen position. However, no significant difference can be observed between blank and Cur NPs-loaded composite hydrogels (Fig. 5g).

Meanwhile, to further understand the level of trauma angiogenesis and inflammatory response, we used CD-31, a transmembrane protein expressed in early angiogenesis, to assess angiogenesis and trauma healing effects. As shown in Fig. 5e and 5h, on day 11, the positive expression of CD-31 in blank or Cur NPs-loaded composite hydrogel-covered wounds is higher than the group in medical gauze ($p < 0.05$), indicating a facilitation for angiogenesis in the healing process. At day 11, the expression of IL-6 is the lowest in the composite hydrogel group loaded with Cur-NPs compared with the medical gauze group ($p < 0.01$). There was also a significant difference between the SF/SA-3 and Cur NPs-loaded SF/SA-3 groups compared with the medical gauze group ($p < 0.01$), indicating a better ability to treat infection (Fig. 5i). These results suggest that SF/SA composite hydrogel application in trabecular tissues can significantly enhance the contraction of trabecular tissues but accelerate wound healing.

3.5 Bacteria-infected wound healing *in vivo*

Many factors, such as bacterial infection, microenvironment imbalance, and cellular

repair dysfunction, can lead to wound deterioration and hinder the healing process [54]. A bacteria-infected wound model is selected to evaluate the wound healing effect of our composite hydrogels (Fig. 6a). The prepared composite hydrogel presented good wound healing after 11 days of healing compared to the control group (Fig. 6b) . Wound area and percentage shrinkage were calculated from the comparison of the healed wound area with the original wound area (Fig. 6c and 6d). On days 2 and 7, the wound sites of Cur-NPs loaded SF/SA hydrogel are smaller ($p < 0.01$) than SF/SA hydrogel and the control groups. Compared to the control group, Cur-NPs loaded SF/SA hydrogel sample presents the smallest ($p < 0.05$) wound areas and highest wound closure among the tested groups after 11 days of treatment, which demonstrates that the Cur-NPs loaded SF/SA hydrogel is the most favorable for wound healing.

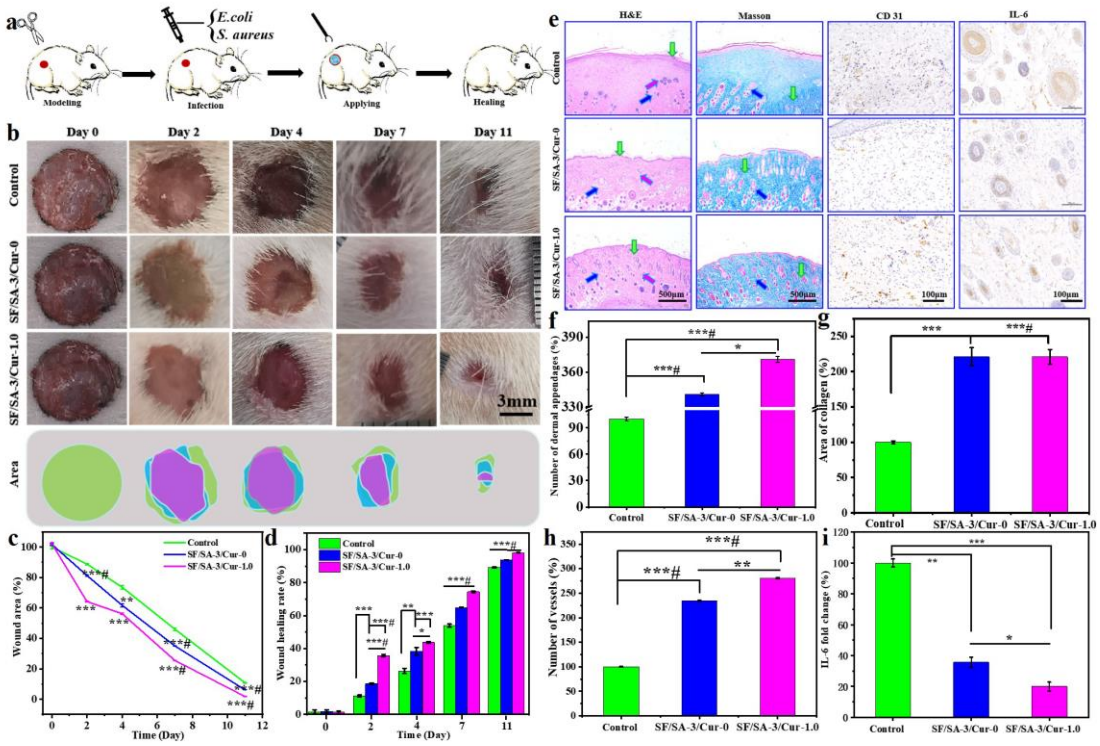

Fig. 6 Schematic illustration of bacteria-infected wound healing using Cur NPs-loaded SF/SA-3 composite hydrogels as dressing (a), bacteria-infected wound images after treated by composite

hydrogels and diagram of wound size during healing (b), wound area (c) and healing rate (d) treated by composite hydrogels at days 0, 2, 4, 7 and 11. H&E and Masson's trichrome staining figures of a wound treated by composite hydrogels (e, inflammatory cells: black arrows; neovascularization: red arrows; hair follicles: green arrows; glands: yellow arrows), number of dermal appendages (f), area of collagen (g), number of vessels (h) and IL-6 secretion levels after treatment (i). * $p < 0.05$, ** $p < 0.01$, *** $p < 0.001$, *** # $p < 0.001$ vs. control group.

Tissue re-epithelialization, collagen deposition, neovascularization, and expression of inflammatory factors can help us to understand the wound healing process more intuitively, as shown in Fig. 6e, where we observed H&E and Masson trichromography of the healed wound tissue. H&E stained images of the control samples showed slight activity of granulation tissue formation and incomplete re-epithelialization. Without severe immunogenic signs and tissue necrosis, the hydrogel samples could induce the formation of numerous dermal appendages in the dermis (Fig. 6f). In addition, collagen fiber formation and collagen formation can be seen by Masson staining of the wound site (Fig. 6e). Higher epithelial tissue regeneration, dermal attachment, collagen deposition, improved inflammation and neointima formation were observed in SF/SA hydrogel samples containing cur - NPs. Collagen deposition percentage (Fig. 6g) and the number of vessels (Fig. 6h) were quantified from Masson stained wound sites using Image J software. From the collagen deposition results (Fig. 6g), the wounds treated with Cur-NPs loaded SF/SA hydrogels had higher collagen deposition that was close to the blank SF/SA hydrogels, and more than 2-fold more collagen deposition than the control group. In addition, it exhibits a higher quantity of vessels in the wound treated with Cur-NPs loaded SF/SA hydrogel (~260%) and blank SF/SA hydrogel (~220%) after 11 days of treatment compared to the control group.

The expression level of IL-6 is ~20% for the Cur-NPs loaded SF/SA hydrogel, which is significantly lower than that of blank SF/SA hydrogel at ~40% using the control group (=100%) as a standard (Fig. 6i). It indicates that incorporating Cur NPs into SF/SA matrices can provide superior compatibility during the *in vivo* wound process, which is consistent with the analysis of compatibility *in vitro*.

4 Conclusions

We have developed a novel antimicrobial Cur-NPs-loaded SF/SA composite hydrogel with adhesive and antimicrobial properties that ccould promote wound healing. The as-prepared composite exhibited excellent biocompatibility and antibacterial abilities against both Gram-negative (*E. coli*) and Gram-positive (*S. aureus*) bacteria *in vitro*. Furthermore, this composite hydrogel showed good tissue adhesive strength which could adhere stably to wounds that are constantly changing in shape due to movement. SF/SA composite hydrogels loaded with Cur-NPs positively interfered with the rate of infected wound healing by improving antimicrobial capacity, collagen deposition, and dermal attachment in a model of total skin defect with or without bacterial infection. Therefore, this study provides a convenient, effective, and safe candidate for designing antimicrobial hydrogels to promote healing of infected wounds.

Author contributions

Y. J., T. L. and R. W. produced composite hydrogels and conducted cell and animal experiments; Y. J., L. R. and G. J. analyzed the results and wrote the draft of manuscript; L. R. and G. J. conceived the idea and designed the experiments; L. N. and A. S. provided suggestions and commented on the manuscript; K. E. Y. and U. E.

A. reviewed and revised the manuscript.

Declaration of Competing Interest

The authors declare that they have no known competing financial interests or personal relationships that could have appeared to influence the work reported in this paper.

Acknowledgments

This research was supported by the Huadong Medicine Joint Funds of the Zhejiang Provincial Natural Science Foundation of China under Grant No. HDMZ23H300020, Natural Science Foundation of Zhejiang Province (LBY20H110001) and National Natural Science Foundation of China (51373155, 51873194).

Reference:

[1] X. Ma, Q. Bian, J. Hu and J. Gao, Stem from nature: Bioinspired adhesive formulations for wound healing, Journal of Controlled Release, 2022, 345, 292-305.

[2] Y. Liang, H. Xu, Z. Li, A. Zhangji and B. Guo, Bioinspired Injectable Self-Healing Hydrogel Sealant with Fault-Tolerant and Repeated Thermo-Responsive Adhesion for Sutureless Post-Wound-Closure and Wound Healing, Nanomicro Lett, 2022, 14, 185.

[3] J. Chen, J. He, Y. Yang, L. Qiao, J. Hu, J. Zhang and B. Guo, Antibacterial adhesive self-healing hydrogels to promote diabetic wound healing, Acta Biomaterialia, 2022, 146, 119-130.

[4] Y. Wang, D. Xiao, L. Quan, H. Chai, X. Sui, B. Wang, H. Xu and Z. Mao, Mussel-inspired adhesive gelatin-polyacrylamide hydrogel wound dressing

loaded with tetracycline hydrochloride to enhance complete skin regeneration, Soft Matter, 2022, 18, 662-674.

[5] L. Zhang, M. Liu, Y. Zhang and R. Pei, Recent Progress of Highly Adhesive Hydrogels as Wound Dressings, Biomacromolecules, 2020, 21, 3966-3983.

[6] P. Li, L. Ruan, G. Jiang, Y. Sun, R. Wang, X. Gao, K. E. Yunusov, U. E. Aharodnikau and S. O. Solomevich, Design of 3D polycaprolactone/epsilon-polylysine-modified chitosan fibrous scaffolds with incorporation of bioactive factors for accelerating wound healing, Acta Biomaterialia, 2022, 152, 197-209.

[7] Y. Hao, C. Yuan, J. Deng, W. Zheng, Y. Ji and Q. Zhou, Injectable Self-Healing First-Aid Tissue Adhesives with Outstanding Hemostatic and Antibacterial Performances for Trauma Emergency Care, ACS Applied Materials & Interfaces, 2022, 14, 16006-16017.

[8] W. Huang, Y. Wang, Y. Chen, Y. Zhao, Q. Zhang, X. Zheng, L. Chen and L. Zhang, Strong and Rapidly Self-Healing Hydrogels: Potential Hemostatic Materials, Advanced Healthcare Materials, 2016, 5, 2813-2822.

[9] J. Liu, Q. Fang, H. Lin, X. Yu, H. Zheng and Y. Wan, Alginate-poloxamer/silk fibroin hydrogels with covalently and physically cross-linked networks for cartilage tissue engineering, Carbohydrate Polymers, 2020, 247, 116593.

[10] Y. Zhao, Z. S. Zhu, J. Guan and S. J. Wu, Processing, mechanical properties and bio-applications of silk fibroin-based high-strength hydrogels, Acta Biomaterialia, 2021, 125, 57-71.

[11] R. Eivazzadeh-Keihan, F. Radinekiyan, H. Madanchi, H. A. M. Aliabadi and A. Maleki, Graphene oxide/alginate/silk fibroin composite as a novel bionanostructure with improved blood compatibility, less toxicity and enhanced mechanical properties, Carbohydr Polymers, 2020, 248, 116802.

[12] R. Wang, L. Ruan, G. Jiang, P. Li, U. E. Aharodnikau, K. E. Yunusov, X. Gao and S. O. Solomevich, Fabrication of Curcumin-Loaded Silk Fibroin and Polyvinyl Alcohol Composite Hydrogel Films for Skin Wound Healing, ACS Appl Bio Mater, 2022, 5, 4400-4412.

[13] L. Liang, T. Liu, Q. Ouyang, S. Li and C. Li, Solid phase synthesis of oxidized sodium alginate-tobramycin conjugate and its application for infected wound healing, Carbohydrate Polymers, 2022, 295, 119843.

[14] J. Zhang, S. Qian, L. Chen, L. Chen, L. Zhao and J. Feng, Highly antifouling double network hydrogel based on poly(sulfobetaine methacrylate) and sodium alginate with great toughness, Journal of Materials Science & Technology, 2021, 85, 235-244.

[15] J. Cai, X. Chen, X. Wang, Y. Tan, D. Ye, Y. Jia, P. Liu and H. Yu, High-water-absorbing calcium alginate fibrous scaffold fabricated by microfluidic spinning for use in chronic wound dressings, RSC Advances, 2018, 8, 39463-39469.

[16] J. Qin, M. Li, M. Yuan, X. Shi, J. Song, Y. He, H. Mao, D. Kong and Z. Gu, Gallium(III)-Mediated Dual-Cross-Linked Alginate Hydrogels with Antibacterial Properties for Promoting Infected Wound Healing, ACS Applied Materials &

Interfaces, 2022, 14, 22426-22442.

[17] C. Luo, A. Guo, Y. Zhao and X. Sun, A high strength, low friction, and biocompatible hydrogel from PVA, chitosan and sodium alginate for articular cartilage, Carbohydr Polymers, 2022, 286, 119268.

[18] X. Liu, X. Qin, Y. Wang and J. Zhong, Physicochemical properties and formation mechanism of whey protein isolate-sodium alginate complexes: Experimental and computational study, Food Hydrocolloids, 2022, 131, 107786.

[19] L. Gao, Y. Zhou, J. Peng, C. Xu, Q. Xu, M. Xing and J. Chang, A novel dual-adhesive and bioactive hydrogel activated by bioglass for wound healing, NPG Asia Materials, 2019, 11, 66.

[20] T. Du, Z. Xiao, J. Cao, L. Wei, C. Li, J. Jiao, Z. Song, J. Liu, X. Du and S. Wang, NIR-activated multi-hit therapeutic Ag_2S quantum dot-based hydrogel for healing of bacteria-infected wounds, Acta Biomaterialia, 2022, 145, 88-105.

[21] S. I. Basha, S. Ghosh, K. Vinothkumar, B. Ramesh, P. H. P. Kumari, K. V. M. Mohan and E. Sukumar, Fumaric acid incorporated Ag/agar-agar hybrid hydrogel: A multifunctional avenue to tackle wound healing, Mater Sci Eng C Mater Biol Appl, 2020, 111, 110743.

[22] T. Xu, Y. Tian, R. Zhang, B. Yu, H. Cong and Y. Shen, Hydrogel vectors based on peptide and peptide-like substances: For treating bacterial infections and promoting wound healing, Applied Materials Today, 2021, 25, 101224.

[23] S. J. Stohs, O. Chen, S. D. Ray, J. Ji, L. R. Bucci and H. G. Preuss, Highly Bioavailable Forms of Curcumin and Promising Avenues for Curcumin-Based

Research and Application: A Review, Molecules, 2020, 25, 1397.

[24] S. Hasanzadeh, M. I. Read, A. R. Bland, M. Majeed, T. Jamialahmadi and A. Sahebkar, Curcumin: an inflammasome silencer, Pharmacol Research, 2020, 159, 104921.

[25] A. Purushothaman, K. S. Teena Rose, J. M. Jacob, R. Varatharaj, K. Shashikala and D. Janardanan, Curcumin analogues with improved antioxidant properties: A theoretical exploration, Food Chemistry, 2022, 373, 131499.

[26] Z. Hussain, H. E. Thu, M. W. Amjad, F. Hussain, T. A. Ahmed and S. Khan, Exploring recent developments to improve antioxidant, anti-inflammatory and antimicrobial efficacy of curcumin: A review of new trends and future perspectives, Materials Science and Engineering C, 2017, 77, 1316-1326.

[27] T. Hu, G.-P. Wu, H. Bu, H. Zhang, W.-X. Li, K. Song and G.-B. Jiang, An injectable, adhesive, and self-healable composite hydrogel wound dressing with excellent antibacterial activity, Chemical Engineering Journal, 2022, 450, 138201.

[28] D. N. Rockwood, R. C. Preda, T. Yucel, X. Wang, M. L. Lovett and D. L. Kaplan, Materials fabrication from Bombyx mori silk fibroin, Nature Protocols, 2011, 6, 1612-31.

[29] R. Ganguly, S. Kumar, A. Kunwar, S. Nath, H. D. Sarma, A. Tripathi, G. Verma, D. P. Chaudhari, V. K. Aswal and J. S. Melo, Structural and therapeutic properties of curcumin solubilized pluronic F127 micellar solutions and hydrogels, Journal of Molecular Liquids, 2020, 314,

[30] R. P. Das, V. V. Gandhi, G. Verma, J. K. Ajish, B. G. Singh and A. Kunwar, Gelatin-lecithin-F127 gel mediated self-assembly of curcumin vesicles for enhanced wound healing, International Journal of Biological Macromolecules, 2022, 210, 403-414.

[31] N. Gao, S. Lü, C. Gao, X. Wang, X. Xu, X. Bai, C. Feng and M. Liu, Injectable shell-crosslinked F127 micelle/hydrogel composites with pH and redox sensitivity for combined release of anticancer drugs, Chemical Engineering Journal, 2016, 287, 20-29.

[32] L. Wang, Z. Chen, Y. Yan, C. He and X. Li, Fabrication of injectable hydrogels from silk fibroin and angiogenic peptides for vascular growth and tissue regeneration, Chemical Engineering Journal, 2021, 418, 129308.

[33] C. C. Liang, A. Y. Park and J. L. Guan, In vitro scratch assay: a convenient and inexpensive method for analysis of cell migration in vitro, Nature Protocols, 2007, 2, 329-333.

[34] B. I. Pinto, N. D. Cruz, O. R. Lujan, C. R. Propper and R. S. Kellar, In Vitro Scratch Assay to Demonstrate Effects of Arsenic on Skin Cell Migration, Journal of Visualized Experiments, 2019, 144,

[35] K. Wang, J. Wang, L. Li, L. Xu, N. Feng, Y. Wang, X. Fei, J. Tian and Y. Li, Synthesis of a novel anti-freezing, non-drying antibacterial hydrogel dressing by one-pot method, Chemical Engineering Journal, 2019, 372, 216-225.

[36] Y. Zhao, X. Liu, X. Peng, Y. Zheng, Z. Cheng, S. Sun, Q. Ding, W. Liu and C. Ding, A poloxamer/hyaluronic acid/chitosan-based thermosensitive hydrogel that

releases dihydromyricetin to promote wound healing, International Journal of Biological Macromolecules, 2022, 216, 475-486.

[37] M. Hamalainen, R. Nieminen, P. Vuorela, M. Heinonen and E. Moilanen, Anti-inflammatory effects of flavonoids: genistein, kaempferol, quercetin, and daidzein inhibit STAT-1 and NF-kappaB activations, whereas flavone, isorhamnetin, naringenin, and pelargonidin inhibit only NF-kappaB activation along with their inhibitory effect on iNOS expression and NO production in activated macrophages, Mediators of Inflammation, 2007, 2007, 45673.

[38] S. Du, N. Zhou, G. Xie, Y. Chen, H. Suo, J. Xu, J. Tao, L. Zhang and J. Zhu, Surface-engineered triboelectric nanogenerator patches with drug loading and electrical stimulation capabilities: Toward promoting infected wounds healing, Nano Energy, 2021, 85, 106004.

[39] P. K. Gavel, D. Dev, H. S. Parmar, S. Bhasin and A. K. Das, Investigations of Peptide-Based Biocompatible Injectable Shape-Memory Hydrogels: Differential Biological Effects on Bacterial and Human Blood Cells, ACS Applied Materials & Interfaces, 2018, 10, 10729-10740.

[40] J. Zhu, G. Jiang, W. Hong, Y. Zhang, B. Xu, G. Song, T. Liu, C. Hong and L. Ruan, Rapid gelation of oxidized hyaluronic acid and succinyl chitosan for integration with insulin-loaded micelles and epidermal growth factor on diabetic wound healing, Materials Science and Engineering: C, 2020, 117, 111273.

[41] S. Jimi, F. De Francesco, G. A. Ferraro, M. Riccio and S. Hara, A Novel Skin Splint for Accurately Mapping Dermal Remodeling and Epithelialization During

Wound Healing, Journal of Cellular Physiology, 2017, 232, 1225-1232.

[42] J. H. Lopes, C. G. França and M. M. Beppu, Development and characterization of membranes derived from SF/GLY/58S hybrid xerogels for the release of inorganic ions as an osteogenic stimulus for bone regeneration, European Polymer Journal, 2019, 116, 425-437.

[43] H. Li, J. Zhang, S. Liu, Y. Yan and X. Li, Consecutive dephosphorylation by alkaline phosphatase-directed in situ formation of porous hydrogels of SF with nanocrystalline calcium phosphate ceramics for bone regeneration, J Mater Chem B, 2020, 8, 9043-9051.

[44] Z. Fan, P. Cheng, Y. Gao, D. Wang, G. Jia, P. Zhang, S. Prakash, Z. Wang and J. Han, Understanding the rheological properties of a novel composite salecan/gellan hydrogels, Food Hydrocolloids, 2022, 123, 107162.

[45] M. V. Ghica, M. Hirjau, D. Lupuleasa and C. E. Dinu-Pirvu, Flow and Thixotropic Parameters for Rheological Characterization of Hydrogels, Molecules, 2016, 21, 786.

[46] S. d. O. Ferreira, T. L. d. A. Montanheiro, L. S. Montagna, L. M. Guerrini and A. P. Lemes, Study of Cellulose Nanocrystals and Zinc Nitrate Hexahydrate Addition in Chitosan Hydrogels, Materials Research, 2019, 22, e20180760.

[47] H. Xie, Q. Bai, F. Kong, Y. Li, X. Zha, L. Zhang, Y. Zhao, S. Gao, P. Li and Q. Jiang, Allantoin-functionalized silk fibroin/sodium alginate transparent scaffold for cutaneous wound healing, International Journal of Biological Macromolecules, 2022, 207, 859-872.

[48] W. Huang, S. Cheng, X. Wang, Y. Zhang, L. Chen and L. Zhang, Noncompressible Hemostasis and Bone Regeneration Induced by an Absorbable Bioadhesive Self-Healing Hydrogel, Advanced Functional Materials, 2021, 31, 2009189.

[49] Y. Shen, X. Wang, Y. Wang, X. Guo, K. Yu, K. Dong, Y. Guo, C. Cai and B. Li, Bilayer silk fibroin/sodium alginate scaffold promotes vascularization and advances inflammation stage in full-thickness wound, Biofabrication, 2022, 14, 035016.

[50] S. R. U. Rehman, R. Augustine, A. A. Zahid, R. Ahmed, M. Tariq and A. Hasan, Reduced Graphene Oxide Incorporated GelMA Hydrogel Promotes Angiogenesis For Wound Healing Applications, International Journal of Nanomedicine, 2019, 14, 9603-9617.

[51] C. Li, C. Mu, W. Lin and T. Ngai, Gelatin Effects on the Physicochemical and Hemocompatible Properties of Gelatin/PAAm/Laponite Nanocomposite Hydrogels, ACS Applied Materials & Interfaces, 2015, 7, 18732-18741.

[52] M. J. Strowitzki, A. S. Ritter, G. Kimmer and M. Schneider, Hypoxia-adaptive pathways: A pharmacological target in fibrotic disease?, Pharmacol Research, 2019, 147, 104364.

[53] S. McDougall, J. Dallon, J. Sherratt and P. Maini, Fibroblast migration and collagen deposition during dermal wound healing: mathematical modelling and clinical implications, Philosophical Trabsactions of The Royal Society A, 2006, 364, 1385-1405.

[54] Q. Zhao, J. Liu, S. Liu, J. Han, Y. Chen, J. Shen, K. Zhu and X. Ma, Multipronged Micelles-Hydrogel for Targeted and Prolonged Drug Delivery in Chronic Wound Infections, ACS Applied Materials & Interfaces, 2022, 14, 46224-46238.